

Tunable spatial mode converters and optical diodes for graphene parallel plate waveguides

VAHID FOROUGHI NEZHAD,^{1,2} ALI HADDADPOUR,^{1,2} AND GEORGIOS VERONIS^{1,2,*}

¹*School of Electrical Engineering and Computer Science, Louisiana State University, Baton Rouge, LA 70803, USA*

²*Center for Computation and Technology, Louisiana State University, Baton Rouge, LA 70803, USA*
**gveronis@lsu.edu*

Abstract: We introduce compact tunable spatial mode converters between the even and odd modes of graphene parallel plate (GPP) waveguides. The converters are reciprocal and are based on spatial modulation of graphene's conductivity. We show that the wavelength of operation of the mode converters can be tuned in the mid-infrared wavelength range by adjusting the chemical potential of a strip on one of the graphene layers of the GPP waveguides. We also introduce optical diodes for GPP waveguides based on a spatial mode converter and a coupler, which consists of a single layer of graphene placed in the middle between the two plates of two GPP waveguides. We find that for both the spatial mode converter and the optical diode the device functionality is preserved in the presence of loss.

© 2016 Optical Society of America

OCIS codes: (130.2790) Guided waves; (260.0260) Physical optics; (240.6680) Surface plasmons.

References and links

1. A. C. Neto, F. Guinea, N. M. Peres, K. S. Novoselov, and A. K. Geim, "The electronic properties of graphene," *Rev. Mod. Phys.* **81**, 109 (2009).
2. A. K. Geim and K. S. Novoselov, "The rise of graphene," *Nature Mater.* **6**, 183–191 (2007).
3. Q. Bao and K. P. Loh, "Graphene photonics, plasmonics, and broadband optoelectronic devices," *ACS Nano* **6**, 3677–3694 (2012).
4. K. S. Novoselov, S. V. Morozov, T. M. G. Mohiaddin, L. A. Ponomarenko, D. C. Elias, R. Yang, I. I. Barbolina, P. Blake, T. J. Booth, D. Jiang, J. Giesbers, E. W. Hill, and A. K. Geim, "Electronic properties of graphene," *Phys. Status Solidi B* **244**, 4106–4111 (2007).
5. L. A. Falkovsky, "Optical properties of graphene," *J. Phys.: Conf. Ser.* **129**, 012004 (2008).
6. M. Jablan, H. Buljan, and M. Soljačić, "Plasmonics in graphene at infrared frequencies," *Phys. Rev. B* **80**, 245435 (2009).
7. S. Thongrattanasiri and F. J. G. de Abajo, "Optical field enhancement by strong plasmon interaction in graphene nanostructures," *Phys. Rev. Lett.* **110**, 187401 (2013).
8. M. Farhat, S. Guenneau, and H. Bağcı, "Exciting graphene surface plasmon polaritons through light and sound interplay," *Phys. Rev. Lett.* **111**, 237404 (2013).
9. J. Christensen, A. Manjavacas, S. Thongrattanasiri, F. H. Koppens, and F. J. García de Abajo, "Graphene plasmon waveguiding and hybridization in individual and paired nanoribbons," *ACS Nano* **6**, 431–440 (2011).
10. W. B. Lu, W. Zhu, H. J. Xu, Z. H. Ni, Z. G. Dong, and T. J. Cui, "Flexible transformation plasmonics using graphene," *Opt. Express* **21**, 10475–10482 (2013).
11. Y. Zhang, J. P. Small, W. V. Pontius, and P. Kim, "Fabrication and electric field dependent transport measurements of mesoscopic graphite devices," arXiv preprint cond-mat/0410314 (2004).
12. K. S. Novoselov, A. K. Geim, S. V. Morozov, D. Jiang, Y. Zhang, S. V. Dubonos, I. V. Grigorieva, and A. A. Firsov, "Electric field effect in atomically thin carbon films," *Science* **306**, 666–669 (2004).
13. K. Novoselov, A. K. Geim, S. Morozov, D. Jiang, M. Katsnelson, I. Grigorieva, S. Dubonos, and A. Firsov, "Two-dimensional gas of massless dirac fermions in graphene," *Nature* **438**, 197–200 (2005).
14. A. Y. Nikitin, F. Guinea, F. García-Vidal, and L. Martín-Moreno, "Edge and waveguide terahertz surface plasmon modes in graphene microribbons," *Phys. Rev. B* **84**, 161407 (2011).
15. X. Zhu, W. Yan, N. A. Mortensen, and S. Xiao, "Bends and splitters in graphene nanoribbon waveguides," *Opt. Express* **21**, 3486–3491 (2013).
16. D. R. Andersen, "Graphene-based long-wave infrared tm surface plasmon modulator," *J. Opt. Soc. Am. B* **27**, 818–823 (2010).
17. D. Correias-Serrano, J. S. Gomez-Diaz, J. Perruisseau-Carrier, and A. Alvarez-Melcon, "Graphene-based plasmonic tunable low-pass filters in the terahertz band," *IEEE Trans. Nanotechnol.* **13**, 1145–1153 (2014).

18. J. Tao, X. Yu, B. Hu, A. Dubrovkin, and Q. J. Wang, "Graphene-based tunable plasmonic bragg reflector with a broad bandwidth," *Opt. Lett.* **39**, 271–274 (2014).
19. Z. Fang, Z. Liu, Y. Wang, P. M. Ajayan, P. Nordlander, and N. J. Halas, "Graphene-antenna sandwich photodetector," *Nano Lett.* **12**, 3808–3813 (2012).
20. L. Wu, H. Chu, W. Koh, and E. Li, "Highly sensitive graphene biosensors based on surface plasmon resonance," *Opt. Express* **18**, 14395–14400 (2010).
21. G. W. Hanson, "Quasi-transverse electromagnetic modes supported by a graphene parallel-plate waveguide," *J. Appl. Phys.* **104**, 084314 (2008).
22. I.-T. Lin and J.-M. Liu, "Optimization of double-layer graphene plasmonic waveguides," *Appl. Phys. Lett.* **105**, 061116 (2014).
23. B. Wang, X. Zhang, X. Yuan, and J. Teng, "Optical coupling of surface plasmons between graphene sheets," *Appl. Phys. Lett.* **100**, 131111 (2012).
24. D. Svintsov, V. Vyurkov, V. Ryzhii, and T. Otsuji, "Voltage-controlled surface plasmon-polaritons in double graphene layer structures," *J. Appl. Phys.* **113**, 053701 (2013).
25. D. Correas-Serrano, J. S. Gomez-Diaz, J. Perruisseau-Carrier, and A. Álvarez-Melcón, "Spatially dispersive graphene single and parallel plate waveguides: Analysis and circuit model," *IEEE Trans. Microwave Theory Tech.* **61**, 4333–4344 (2013).
26. K. J. Ooi, H. S. Chu, P. Bai, and L. K. Ang, "Electro-optical graphene plasmonic logic gates," *Opt. Lett.* **39**, 1629–1632 (2014).
27. P.-Y. Chen, C. Argyropoulos, and A. Alu, "Terahertz antenna phase shifters using integrally-gated graphene transmission-lines," *IEEE Trans. Antennas Propag.* **61**, 1528–1537 (2013).
28. H. Li, L. Wang, Z. Huang, B. Sun, X. Zhai, and X. Li, "Mid-infrared, plasmonic switches and directional couplers induced by graphene sheets coupling system," *Europhys. Lett.* **104**, 37001 (2013).
29. H. Iizuka and S. Fan, "Deep subwavelength plasmonic waveguide switch in double graphene layer structure," *Appl. Phys. Lett.* **103**, 233107 (2013).
30. D. Dai, J. Wang, and S. He, "Silicon multimode photonic integrated devices for on-chip mode-division-multiplexed optical interconnects (invited review)," *Prog. Electromagn. Res.* **143**, 773–819 (2013).
31. D. A. B. Miller, "All linear optical devices are mode converters," *Opt. Express* **20**, 23985–23993 (2012).
32. W. Liu, D. Yang, G. Shen, H. Tian, and Y. Ji, "Design of ultra compact all-optical XOR, XNOR, NANAD and OR gates using photonic crystal multi-mode interference waveguides," *Opt. Laser Technol.* **50**, 55–64 (2013).
33. V. Liu, D. A. B. Miller, and S. Fan, "Ultra-compact photonic crystal waveguide spatial mode converter and its connection to the optical diode effect," *Opt. Express* **20**, 28388–28397 (2012).
34. D. Correas-Serrano, J. S. Gomez-Diaz, D. L. Sounas, Y. Hadad, A. Alvarez-Melcon, and A. Alù, "Nonreciprocal graphene devices and antennas based on spatiotemporal modulation," *IEEE Antennas Wireless Propag. Lett.* **15**, 1529–1533 (2016).
35. S. Feng and Y. Wang, "Unidirectional light propagation characters of the triangular-lattice hybrid-waveguide photonic crystals," *Opt. Mater.* **35**, 1455–1460 (2013).
36. A. Khavasi, M. Rezaei, A. P. Fard, and K. Mehrany, "A heuristic approach to the realization of the wide-band optical diode effect in photonic crystal waveguides," *J. Opt.* **15**, 075501 (2013).
37. H. Ye, D. Wang, Z. Yu, J. Zhang, and Z. Chen, "Ultra-compact broadband mode converter and optical diode based on linear rod-type photonic crystal waveguide," *Opt. Express* **23**, 9673–9680 (2015).
38. Y.-T. Hung, C.-B. Huang, and J.-S. Huang, "Plasmonic mode converter for controlling optical impedance and nanoscale light-matter interaction," *Opt. Express* **20**, 20342–20355 (2012).
39. X.-T. Kong, Z.-B. Li, and J.-G. Tian, "Mode converter in metal-insulator-metal plasmonic waveguide designed by transformation optics," *Opt. Express* **21**, 9437–9446 (2013).
40. J. Kim, S.-Y. Lee, H. Park, K. Lee, and B. Lee, "Reflectionless compact plasmonic waveguide mode converter by using a mode-selective cavity," *Opt. Express* **23**, 9004–9013 (2015).
41. D. Ohana and U. Levy, "Mode conversion based on dielectric metamaterial in silicon," *Opt. Express* **22**, 27617–27631 (2014).
42. B. Oner, K. Üstün, H. Kurt, A. Okyay, and G. Turhan-Sayan, "Large bandwidth mode order converter by differential waveguides," *Opt. Express* **23**, 3186–3195 (2015).
43. L. Feng, M. Ayache, J. Huang, Y.-L. Xu, M.-H. Lu, Y.-F. Chen, Y. Fainman, and A. Scherer, "Nonreciprocal light propagation in a silicon photonic circuit," *Science* **333**, 729–733 (2011).
44. L. H. Frandsen, Y. Elesin, L. F. Frellsen, M. Mitrovic, Y. Ding, O. Sigmund, and K. Yvind, "Topology optimized mode conversion in a photonic crystal waveguide fabricated in silicon-on-insulator material," *Opt. Express* **22**, 8525–8532 (2014).
45. G. W. Hanson, "Dyadic green's functions for an anisotropic, non-local model of biased graphene," *IEEE Trans. Antennas Propag.* **56**, 747–757 (2008).
46. G. D. Bouzianas, N. V. Kantartzis, T. V. Yioultis, and T. D. Tsiboukis, "Consistent study of graphene structures through the direct incorporation of surface conductivity," *IEEE Trans. Magn.* **50**, 161–164 (2014).
47. V. Nayyeri, M. Soleimani, and O. M. Ramahi, "Modeling graphene in the finite-difference time-domain method using a surface boundary condition," *IEEE Trans. Antennas Propag.* **61**, 4176–4182 (2013).
48. K. Qin, B. Xiao, and R. Sun, "Mode analysis and research on graphene nanoribbons parallel-plate waveguide," *IET*

- Micro & Nano Letters **10**, 558–560 (2015).
49. M. Liu, X. Yin, and X. Zhang, “Double-layer graphene optical modulator,” *Nano Lett.* **12**, 1482–1485 (2012).
50. J. Gomez-Diaz, C. Moldovan, S. Capdevila, J. Romeu, L. Bernard, A. Magrez, A. Ionescu, and J. Perruisseau-Carrier, “Self-biased reconfigurable graphene stacks for terahertz plasmonics,” *Nat. Commun.* **6**, 6334 (2015).
51. J. Cai, P. Ruffieux, R. Jaafar, M. Bieri, T. Braun, S. Blankenburg, M. Muoth, A. P. Seitsonen, M. Saleh, X. Feng, K. Mullen, and R. Fasel, “Atomically precise bottom-up fabrication of graphene nanoribbons,” *Nature* **466**, 470–473 (2010).
52. S. Masubuchi, M. Ono, K. Yoshida, K. Hirakawa, and T. Machida, “Fabrication of graphene nanoribbon by local anodic oxidation lithography using atomic force microscope,” *Appl. Phys. Lett.* **94**, 082107 (2009).

1. Introduction

Graphene, which is a two-dimensional version of graphite, has been shown to have many interesting electronic and optical properties [1–5]. The ability of layers of graphene to support surface plasmon polaritons has opened a new path for researchers to manipulate light at subwavelength scales [6–8]. Compared to conventional plasmonic materials, such as silver or gold, surface plasmons on graphene exhibit several important features including tunability [9], low-loss [3], and extreme mode confinement [10]. In addition, the conductivity and transport characteristics of graphene can be tuned using either electrostatic or magnetostatic gating, or via chemical doping [11–13]. Because of these properties, graphene is an excellent candidate for designing novel subwavelength plasmonic devices. Various structures exploiting plasmons on graphene have been proposed including waveguides [14, 15], modulators [16], filters [17, 18], photodetectors [19], and sensors [20].

In addition, the coupling between graphene plates has been investigated [21–25], and it has been demonstrated that coupled graphene plates, otherwise known as graphene parallel plate (GPP) waveguides, could be employed in designing different structures such as logic gates [26], phase shifters [27], and optical switches [28, 29]. Since GPP waveguides support multiple modes [23], it is important to develop spatial mode converters for such waveguides. The ability to manipulate optical spatial modes in integrated photonic circuits has significant importance due to its potential applications in mode-division multiplexing, efficient waveguide coupling, and all-optical logic gates and diodes [30–33]. Correas-Serrano *et al.* recently introduced plasmonic isolators for THz waves based on GPP waveguides. These devices are based on unidirectional mode conversion which is achieved through the spatiotemporal modulation of graphene’s conductivity [34]. Several different mode converters based on photonic crystal, silicon, metal-insulator-metal, and nanowire waveguides have also been proposed, and their connection to multiplexing and all-optical diodes have been investigated [33, 35–42]. Recently, an all-optical modal isolator based on a multimode silicon waveguide was designed and fabricated by Feng *et al.* [43]. In addition, Frandsen *et al.* designed and experimentally verified a topology optimized mode converter, which converts the fundamental even mode of a dispersion engineered photonic crystal waveguide to the higher order odd mode [44].

In this paper, we first introduce a spatial mode converter between the even and odd modes of a GPP waveguide, based on modifying the chemical potential of a strip on one of the graphene layers of the waveguide. We find that using a chemical potential profile that corresponds to a piecewise approximation of a triangular envelope reduces reflection in the mode converter to almost zero in a broad wavelength range. In addition, modifying the chemical potential of a strip on both the upper and lower graphene plates leads to larger maximum conversion efficiency. We show that the wavelength of operation of the mode converter can be tuned in the mid-infrared wavelength range simply by adjusting the chemical potential of the graphene strip. We also introduce an optical diode for GPP waveguides based on the mode converter and a coupler, which consists of a single layer of graphene placed in the middle between the two plates of two GPP waveguides. We find that for both the spatial mode converter and the optical diode the device functionality is preserved in the presence of loss.

2. Mode converter

Figure 1 shows the schematic of a typical mode converter along with its scattering matrix. We use A and B to denote the even and odd modes, respectively, to the left of the converter. Similarly, we use C and D to denote the even and odd modes, respectively, to the right of the converter. The scattering matrix S of the converter relates the amplitudes of the outgoing modes to the amplitudes of the ingoing modes [33]. Since we are interested in the power conversion between different modes, we also define $T_{ij} \equiv |S_{ij}|^2$. Thus, the elements of matrix T represent the power coupling efficiency between different modes. For an ideal converter $T_{AD} = T_{DA} = T_{BC} = T_{CB} = 1$, while all other matrix elements are equal to zero. Thus, the scattering matrix of an ideal converter is an anti-diagonal matrix with entries that are all equal to one. Due to the fact that the device is reciprocal, one only needs to specify the first two rows of matrix T to completely determine this matrix.

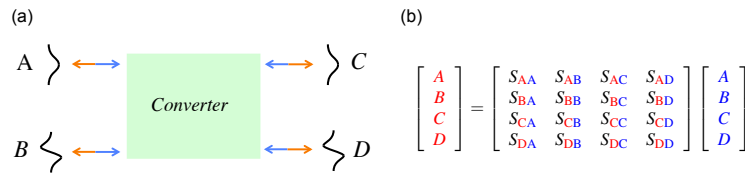


Fig. 1. (a) The schematic of a typical mode converter. We use the letters A, B, C, and D to denote different modes. The blue and red arrows correspond to input and output in each mode, respectively. (b) The scattering matrix S of the converter relates the amplitudes of the outgoing modes (denoted in red) to the amplitudes of the ingoing modes (denoted in blue).

We first briefly review the material properties of graphene. Based on the Kubo formula the surface conductivity of graphene in the absence of magnetic field can be written as follows [45]

$$\sigma(\omega, \mu_c, \tau, T) = \sigma_{\text{intra}} + \sigma_{\text{inter}}, \quad (1)$$

where

$$\sigma_{\text{intra}} = \frac{\tau e^2 k_B T}{\pi \hbar^2 (j\omega\tau + 1)} \left\{ \frac{\mu_c}{k_B T} + 2 \ln \left[\exp\left(-\frac{\mu_c}{k_B T}\right) + 1 \right] \right\}, \quad (2)$$

and

$$\sigma_{\text{inter}} = \frac{-je^2}{4\pi\hbar} \ln \left[\frac{2|\mu_c| - \hbar(\omega - j\tau^{-1})}{2|\mu_c| + \hbar(\omega - j\tau^{-1})} \right]. \quad (3)$$

The first and second terms in Eq. (1) are associated with intraband and interband contributions, respectively. The parameters μ_c , ω , τ , k_B , \hbar , T , $-e$ are the chemical potential, angular frequency, phenomenological carrier relaxation time, Boltzmann constant, reduced Planck constant, temperature, and electron charge, respectively. For the frequency range of interest in this paper we have $\hbar\omega \gg k_B T$ so that $\sigma_{\text{intra}} \gg \sigma_{\text{inter}}$. The dependence of the carrier density of undoped graphene n_s on the external voltage V_g is given by [45]

$$n_s = \frac{V_g \epsilon_0 \epsilon_r}{ed}, \quad (4)$$

where ϵ_0 is the dielectric permittivity of free space, ϵ_r is the relative dielectric permittivity of the intermediate layer (the layer between graphene and the electrode where the voltage V_g is applied), and d is the thickness of the intermediate layer. The chemical potential can be calculated via [45]

$$n_s = \frac{2}{\pi \hbar^2 v_f^2} \int_0^\infty \epsilon [f_d(\epsilon) - f_d(\epsilon + 2\mu_c)] d\epsilon. \quad (5)$$

The function $f_d(\epsilon) = [1 + \exp(\frac{\epsilon - \mu_c}{k_B T})]^{-1}$ is the Fermi function, and v_f is the Fermi velocity. Thus, based on Eqs. (4) and (5), the chemical potential of graphene can be easily adjusted by applying an external voltage. The negative imaginary part of σ in the infrared wavelength range, enables graphene to support surface plasmons.

The dispersion relation of the TM modes supported by a single-layer graphene sheet is given by [6]

$$\frac{\epsilon_{r1}}{k_1} + \frac{\epsilon_{r2}}{k_2} = j \frac{\sigma}{\omega \epsilon_0}, \quad (6)$$

where

$$k_i = \sqrt{\beta^2 - k_0^2 \epsilon_{ri}}, \quad (7)$$

ϵ_{r1} and ϵ_{r2} are the relative dielectric permittivities of the media surrounding the graphene layer, $k_0 = \omega / c$ is the free space wavenumber, and β is the propagation constant of the single-layer graphene.

In this paper, all graphene sheets are modeled via a two-dimensional surface boundary condition with surface conductivity $\sigma = \sigma_{\text{intra}}$ using the two-dimensional finite-difference time-domain (2D-FDTD) method [46, 47]. We use our in-house FDTD code with perfectly matched layer (PML) absorbing boundary conditions at all boundaries of the simulation domain [47]. The typical dimensions of the simulation domain that we use for the proposed mode converters are $2 \mu\text{m}$ in the x direction, and $1 \mu\text{m}$ in the z direction (Fig. 2). We use a spatial grid size of 2 nm in FDTD which we found to be sufficient for the convergence of numerical results.

GPP waveguides consist of two layers of graphene that are brought close together. Due to the proximity of the two layers, their modes couple. GPP waveguides therefore support a symmetric (even) and an anti-symmetric (odd) mode [23]. Here we propose a structure based on GPP waveguides that operates as a mode converter between the even and odd modes of GPP waveguides. The principle of the device operation is based on the fact that the odd and even modes can be thought of as in-phase and π out-of-phase interactions, respectively, between the surface plasmons propagating on the upper and lower graphene layers. Assuming that the coupling between the two layers is weak, to convert one mode into the other, one needs to create an odd multiple of π phase shift between them. To achieve the required phase shift, we modify the chemical potential μ_c on a strip on one of the graphene layers by applying an external voltage or by chemically doping it. The schematic of the converter is shown in Fig. 2. The strip with the different chemical potential is shown in red. If the coupling between the two graphene layers is weak, the structure can be treated as two weakly coupled single-layer waveguides and the condition for the required phase shift can be approximated as

$$\beta_s L - \beta_g L = (2m - 1)\pi, \quad (8)$$

where β_s and β_g are the propagation constants of surface plasmons propagating on single-layer graphene waveguides with chemical potential μ_{cs} and μ_{cg} , respectively, which can be calculated using Eqs. (6) and (7). L is the length of the strip, and m is an integer number. Therefore, for a given μ_{cg} , by appropriate choices of μ_{cs} and L one can obtain the phase shift required for the conversion process.

To simplify the design procedure, we first assume that the graphene layers are lossless ($\tau \rightarrow \infty$). The effect of loss will be considered later. We also assume that all graphene layers are suspended in air and that the temperature is $T = 300 \text{ K}$.

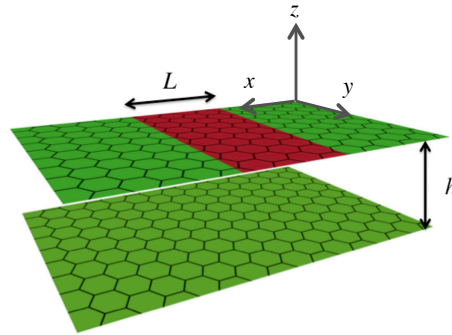


Fig. 2. Schematic of a spatial mode converter consisting of two parallel layers of graphene with chemical potential μ_{cg} , and a strip of length L with chemical potential μ_{cs} , shown in red.

Figure 3(a) shows the profile of the chemical potential of the upper graphene layer. For such a profile Fig. 3(b) shows the transmission spectra from mode A to modes C and D, as well as the reflection spectra to modes A and B calculated with FDTD. Even though we only show here the conversion efficiency from mode A to mode D, the other three conversion processes (D to A, B to C, and C to B) have identical spectra due to reciprocity and the symmetry of the structure [33]. We observe that for the given structure parameters, the calculated conversion efficiency from mode A to mode D is maximized at $\lambda = 10.35 \mu\text{m}$. In addition, the condition for the required phase shift for maximum conversion efficiency [Eq. (8)] with $m=1$ is satisfied for $\lambda = 10.25 \mu\text{m}$, which is in good agreement with the numerical simulation result. We also observe that, due to the abrupt change in the chemical potential on the upper plate, the conversion from mode A to mode D at the optimum wavelength $\lambda = 10.35 \mu\text{m}$ is not complete.

One of the methods to reduce the reflection in such a structure is to modify the chemical potential profile of the strip [27]. Here, we use a chemical potential profile that corresponds to a piecewise approximation of a triangular envelope as shown in Fig. 4(a) with minimum potential of μ_{cm} . Modifying the chemical potential profile of the strip reduces the reflection coefficients of the mode converter to almost zero in a broad wavelength range [Fig. 4(b)]. The profile of H_z shown in the inset of Fig. 4(b), corresponds to mode conversion with $\sim 99\%$ efficiency at a wavelength of $\lambda = 10.1 \mu\text{m}$. In addition, the conversion efficiency is more than 90% in a wavelength range extending from $\lambda_1 = 9.3 \mu\text{m}$ to $\lambda_2 = 11.2 \mu\text{m}$.

The condition for the optimum mode conversion for the structure with modified chemical potential profile can be approximated as

$$\sum_{i=1}^N \beta_i d_i - \beta_g L = (2m - 1)\pi, \quad (9)$$

where d_i is the length of the i^{th} segment of the strip with corresponding chemical potential μ_{ci} , N is the number of segments, and $L = \sum_{i=1}^N d_i$ is the total length of the strip. In addition, β_i is the propagation constant of the surface plasmon mode propagating on a single-layer graphene waveguide with chemical potential μ_{ci} , which can be calculated using Eqs. (6) and (7). For the profile shown in Fig. 4(a), $d_i = 50 \text{ nm}$ for $i \neq 4$, and $d_4 = 100 \text{ nm}$. Using Eq. (9), the wavelength which corresponds to maximum conversion efficiency is calculated to be $\lambda_{\text{opt}} = 10.24 \mu\text{m}$, which is in good agreement with the optimum wavelength obtained from the FDTD numerical simulations ($\lambda = 10.1 \mu\text{m}$).

The wavelength of operation of the mode converter can be tuned by adjusting the chemical potential of the graphene strip. Figure 5(a) shows the conversion efficiency for different values

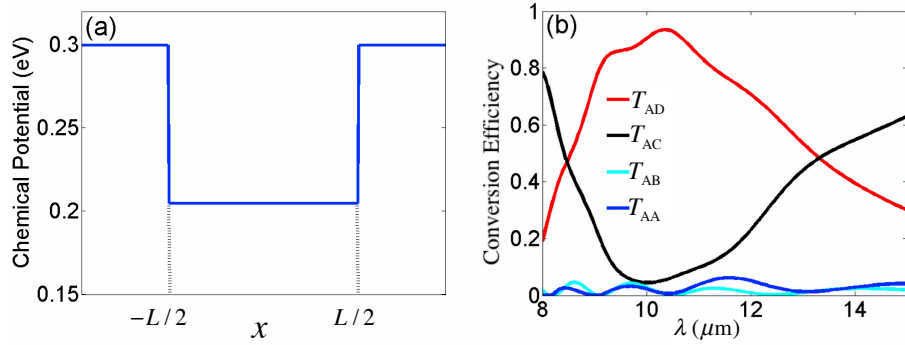


Fig. 3. (a) Profile of the chemical potential of the upper graphene layer in the spatial mode converter shown in Fig. 2. (b) Transmission spectra from mode A to modes C and D, and reflection spectra to modes A and B calculated with FDTD for the mode converter shown in Fig. 2 with chemical potential profile as in Fig. 3(a), and $\mu_{cg} = 0.3$ eV, $\mu_{cs} = 0.205$ eV, $h = 150$ nm, $L = 400$ nm. The graphene layers are assumed to be lossless.

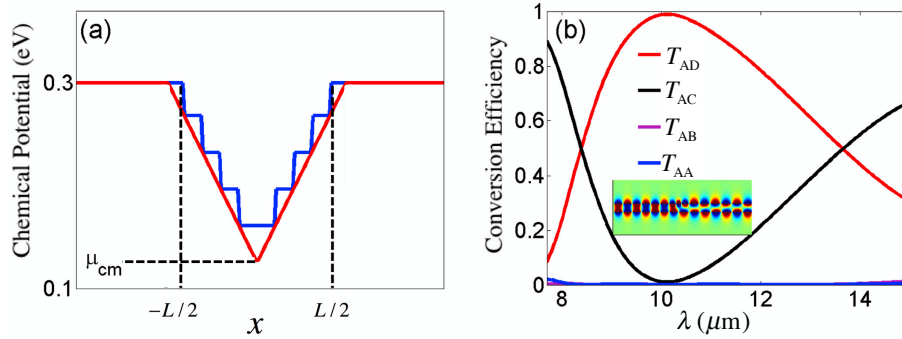


Fig. 4. (a) Chemical potential profile of the graphene strip in the spatial mode converter shown in Fig. 2. The profile corresponds to a piecewise approximation with a step size of 50 nm of a triangular envelope with minimum potential of μ_{cm} . (b) Transmission spectra from mode A to modes C and D, and reflection spectra to modes A and B calculated with FDTD for the mode converter shown in Fig. 2 with chemical potential profile as in Fig. 4(a), and $\mu_{cm} = 0.127$ eV. All other parameters are as in Fig. 3(b). The magnetic field profile at $\lambda = 10.1$ μm shown in the inset demonstrates the complete conversion of the even mode A incident from the left into the odd mode D propagating to the right, and vice versa.

of the minimum potential μ_{cm} of the triangular envelope [Fig. 4(a)]. The profile applied here is as in Fig. 4(a). We observe that the wavelength which corresponds to maximum conversion efficiency can be tuned simply by adjusting the minimum value μ_{cm} of the applied profile of the chemical potential. As mentioned above, the chemical potential of graphene can in turn be adjusted through the external applied voltage. We observe that, as μ_{cm} decreases, the wavelength of maximum conversion efficiency λ_{opt} increases [Fig. 5(a)]. As before, we use Eq. (9) to calculate the wavelength which corresponds to maximum conversion efficiency λ_{opt} as a function of μ_{cm} , and find that it is in good agreement with the optimum wavelength obtained from the FDTD numerical simulations [Fig. 5(b)]. In the Appendix we also derive a relationship between the wavelength corresponding to maximum conversion efficiency λ_{opt} and the minimum potential μ_{cm} . We found that this relationship gives results indistinguishable from those obtained using Eq. (9).

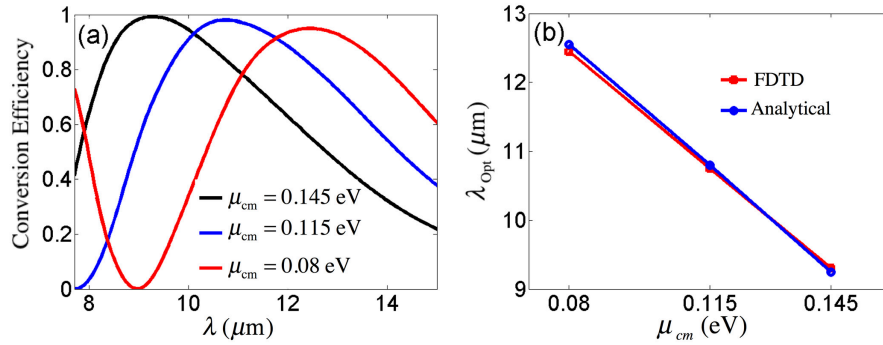


Fig. 5. (a) Conversion efficiency spectra calculated with FDTD for the mode converter shown in Fig. 2 with chemical potential profile as in Fig. 4(a) for different values of the minimum potential μ_{cm} of the triangular envelope. Results are shown for $\mu_{cm} = 0.145$ eV, $\mu_{cm} = 0.115$ eV, and $\mu_{cm} = 0.08$ eV. All other parameters are as in Fig. 3(b). (b) The wavelength which corresponds to maximum conversion efficiency λ_{opt} as a function of μ_{cm} calculated using Eq. (9) (blue line), and FDTD (red line). All other parameters are as in Fig. 5(a).

We also observe that the maximum conversion efficiency slightly decreases, as μ_{cm} decreases [Fig. 5(a)]. The decrease in the maximum conversion efficiency is due to stronger coupling between the graphene plates. Several factors could lead to increased coupling between the sheets including increasing the wavelength, decreasing the distance between the plates, and increasing the chemical potential of the plates [23]. Under the strong coupling condition, the system can no longer be treated as two weakly coupled single-layer waveguides. To overcome this issue, we modify the chemical potential of a strip on both the upper and lower graphene plates [Fig. 6(a)]. As the chemical potential of the lower plate is reduced, the coupling between the modes supported by the two plates decreases. The condition for the optimum mode conversion for the structure with strips with modified chemical potential on both the upper and lower graphene plates [Fig. 6(a)], assuming similar profiles on both plates, can be approximated as

$$\sum_{i=1}^N (\beta_{ui} - \beta_{di})d_i = (2m - 1)\pi, \quad (10)$$

where d_i is the length of the i^{th} segment of the strips with corresponding chemical potentials μ_{cui} and μ_{cdi} for the upper and lower plates, respectively. In addition, β_{ui} (β_{di}) is the propagation constant of the surface plasmon mode propagating on a single-layer graphene waveguide with chemical potential μ_{cui} (μ_{cdi}), which can be calculated using Eqs. (6) and (7). In order to compare the performance of the double strip converter with the single strip converter, the chemical potential profile parameters are chosen so that the wavelength which corresponds to maximum conversion efficiency λ_{opt} is the same in both cases. The minimum potential for the single strip converter is set to be $\mu_{cm} = 0.08$ eV. For the double strip case the minimum potentials of the upper and lower strips are set to be $\mu_{cmu} = 0.05$ eV and $\mu_{cmd} = 0.19$ eV, respectively. The strip length is $L = 400$ nm and the plate separation is $h = 150$ nm in both cases. We observe that the double strip converter achieves larger maximum conversion efficiency compared to the single strip converter [Fig. 6(b)]. Thus, in the case of strong coupling between the graphene plates, which limits the maximum conversion efficiency, the double strip converter can be used to increase the efficiency.

As mentioned above, increasing the chemical potential of the graphene plates or decreasing the distance between the plates leads to stronger coupling between them, and therefore de-

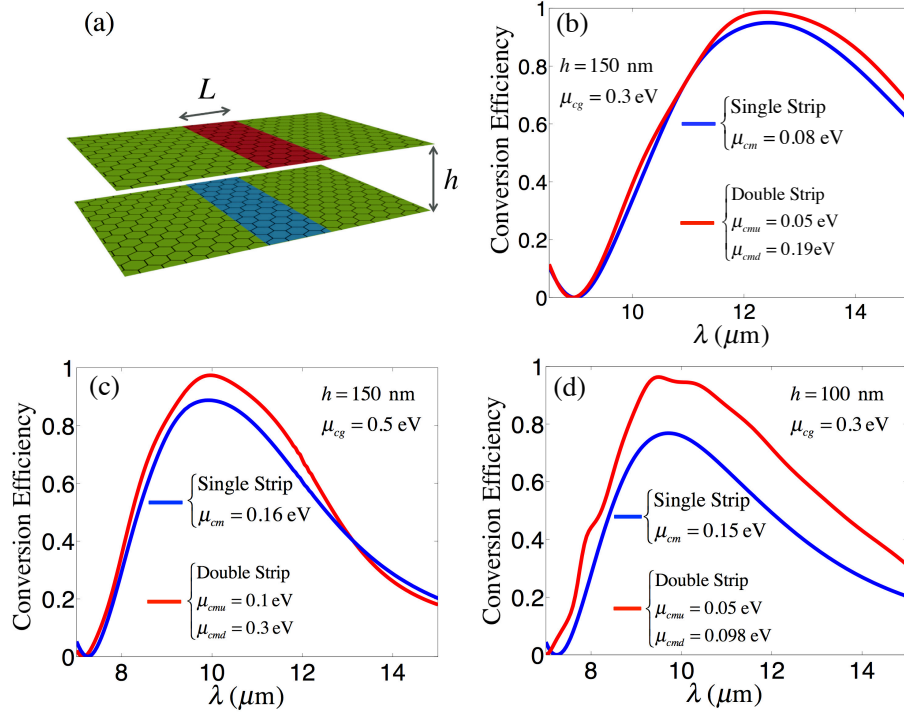


Fig. 6. (a) Schematic of the double strip spatial mode converter. It consists of two parallel layers of graphene with strips with modified chemical potential on both the upper and lower graphene plates, shown in red and blue, respectively. (b) Conversion efficiency spectra calculated with FDTD for the single strip (Fig. 2) and double strip [Fig. 6(a)] mode converters with chemical potential profile as in Fig. 4(a). The minimum potential for the single strip converter is set to be $\mu_{cm} = 0.08$ eV. For the double strip case the minimum potentials of the upper and lower strips are set to be $\mu_{cmu} = 0.05$ eV and $\mu_{cmd} = 0.19$ eV, respectively. The strip length is $L = 400$ nm and the plate separation is $h = 150$ nm in both cases. All other parameters are as in Fig. 3(b). (c) Same as in (b), except that $L = 500$ nm, $\mu_{cg} = 0.5$ eV, the minimum potential for the single strip converter is set to be $\mu_{cm} = 0.16$ eV, and for the double strip case the minimum potentials of the upper and lower strips are set to be $\mu_{cmu} = 0.1$ eV and $\mu_{cmd} = 0.3$ eV, respectively. (d) Same as in (b), except that $L = 500$ nm, $h = 100$ nm, the minimum potential for the single strip converter is set to be $\mu_{cm} = 0.15$ eV, and for the double strip case the minimum potentials of the upper and lower strips are set to be $\mu_{cmu} = 0.05$ eV and $\mu_{cmd} = 0.098$ eV, respectively.

creased maximum conversion efficiency. We now consider a structure with increased chemical potential of $\mu_{cg} = 0.5$ eV. The parameters of the mode converter are adjusted in such a way that the wavelength of maximum conversion efficiency is $\lambda_{opt} = 10$ μm . When the single strip converter is used, the maximum conversion efficiency for $\mu_{cg} = 0.5$ eV [Fig. 6(c)] is reduced compared to the one for $\mu_{cg} = 0.3$ eV [Fig. 6(b)], due to the stronger coupling between the graphene plates. As before, to overcome this issue we use the double strip converter with its parameters adjusted so that the wavelength of maximum conversion efficiency λ_{opt} is the same as the one of the single strip converter. Once again, we observe that the double strip converter achieves larger maximum conversion efficiency compared to the single strip converter [Fig. 6(c)].

We also consider a structure with decreased distance between the graphene plates of $h = 100$

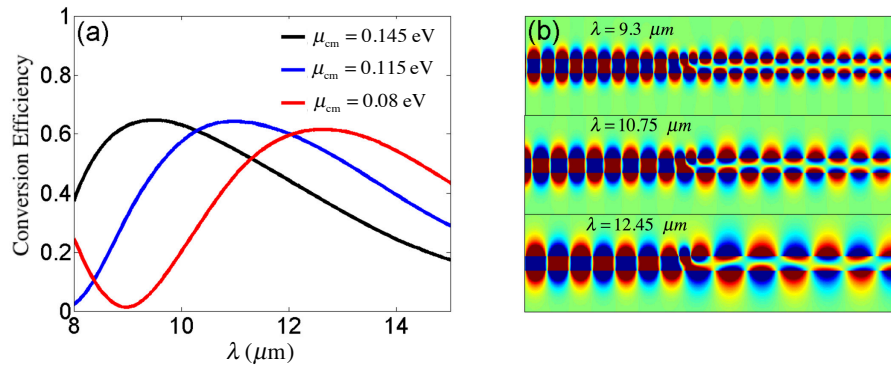


Fig. 7. (a) Conversion efficiency spectra calculated with FDTD for the mode converter shown in Fig. 2 with chemical potential profile as in Fig. 4(a) for different values of the minimum potential μ_{cm} of the triangular envelope, when the effect of material loss in graphene is included. All other parameters are as in Fig. 5(a). (b) Magnetic field profiles for the converters with $\mu_{cm} = 0.145$ eV (top figure), $\mu_{cm} = 0.115$ eV (middle figure), and $\mu_{cm} = 0.08$ eV (bottom figure). In each case the profile is shown at the wavelength which corresponds to maximum conversion efficiency λ_{opt} .

nm. As before, we compare the performance of single strip and double strip converters, when their parameters are adjusted so that the wavelength of maximum conversion efficiency λ_{opt} is the same in both cases. When the single strip converter is used, the maximum conversion efficiency for $h = 100$ nm [Fig. 6(d)] is significantly reduced compared to the one for $h = 150$ nm [Fig. 6(b)], due to the stronger coupling between the graphene plates. However, use of the double strip converter for $h = 100$ nm leads to greatly enhanced maximum conversion efficiency [Fig. 6(d)], which approaches the one for $h = 150$ nm [Fig. 6(b)].

Finally, the effect of the loss on the structure is investigated by setting the phenomenological carrier relaxation time τ [Eqs. (1)-(3)] to be $\tau = \mu\mu_c/(ev_f^2)$, where $\mu = 10^4 \text{ cm}^2\text{V}^{-1}\text{s}^{-1}$ is the carrier mobility, and $v_f = 10^6 \text{ ms}^{-1}$ is the Fermi velocity [6]. The lossless case results [Fig. 5(a)] can be compared to the lossy case results shown in Fig. 7(a). When the effect of loss is included, there is absorption in the mode converter, which causes the transmission and consequently the conversion efficiency to decrease. It should be noted that the reduction of the conversion efficiency from mode A to mode D is solely due to absorption. We found that the maxima of the transmission spectra from mode A to mode C, and of the reflection spectra from mode A to modes A and B are less than 1%. The H_z profiles shown in Fig. 7(b) demonstrate that, even in the presence of loss, mode A, which is even, is converted to mode D, which is odd, with negligible transmission to mode C and reflection to modes A and B.

3. Optical diode

An ideal optical diode is a device which allows the complete transmission of one mode in one direction, while entirely reflects all other modes entering the device from the same direction. If the same mode is sent from the other direction, it is completely reflected [33]. Figure 8 shows the schematic of the proposed optical diode. The device includes a mode converter as the one analyzed in the previous section (shown in red color), and a coupler, which consists of a single layer of graphene placed in the middle between the two plates of two GPP waveguides. This structure is an ideal optical diode if mode A from the left (Fig. 1) is completely transmitted to mode D on the right, while mode B from the left is completely reflected into the same mode B on the left. In addition, mode D from the right is completely transmitted to mode A on the

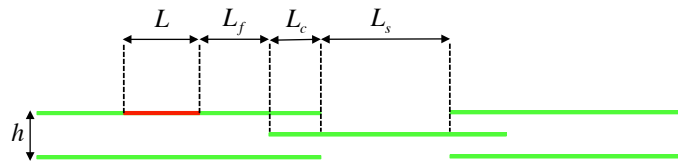


Fig. 8. Schematic of an optical diode consisting of two GPP waveguides, which includes a mode converter on the left GPP waveguide (shown in red color), and a coupler, which consists of a single layer of graphene placed in the middle between the two plates of the two GPP waveguides.

left, while mode C from the right is completely reflected into the same mode C on the right [33]. Similar to the analysis of the mode converter, we first assume that all graphene layers are lossless ($\tau \rightarrow \infty$), while the effect of loss is considered later. We emphasize that the proposed optical diode is a fully reciprocal device [33].

The coupling between the GPP waveguides and the middle single graphene layer enables the transmission of light from one side of the structure to the other. The single graphene layer supports an antisymmetric (odd) mode. As mentioned above, GPP waveguides support a symmetric (even) and an anti-symmetric (odd) mode. Thus, if the even mode of the GPP waveguide is incident on the coupler, the coupling between the GPP waveguide and the single graphene layer is zero, due to the complete field profile mismatch. In contrast, there is strong coupling, if the odd mode of the GPP waveguide is incident on the coupler. This different coupling behavior along with the existence of the mode converter on side of the device enable it to perform as an optical diode. When the even mode of the GPP waveguide is incident from the left, it is converted into the odd mode of the GPP waveguide through the mode converter. The odd mode of the GPP waveguide on the left is in turn strongly coupled to the mode of the single graphene layer, which then couples to the odd mode of the GPP waveguide on the right. On the other hand, when the odd mode of the GPP waveguide is incident from the left, it is converted into the even mode of the GPP waveguide through the mode converter. However, as mentioned above, the even mode of the GPP waveguide on the left cannot couple to the mode of the single graphene layer, and is therefore reflected. Since the right GPP waveguide does not include a mode converter, when the even (odd) mode of the GPP waveguide is incident from the right, it will be reflected (transmitted). The distance between the mode converter on the left GPP waveguide and the coupler L_f (Fig. 8) should be large enough, so that the mode on the output of the converter is fully formed. On the other hand, increasing the size of the device results in increased insertion loss. The length of the coupler L_c (Fig. 8) has to be chosen so that the coupling, when the odd mode of the GPP waveguide is incident on the coupler, is maximized at the wavelength λ_{opt} which corresponds to maximum conversion efficiency of the mode converter.

The coupler length L_c which leads to maximum coupling can be estimated as $L_c = \pi / (2|\beta_{\text{even}} - \beta_{\text{odd}}|)$ [28], where β_{even} and β_{odd} are the propagation constants of the even and odd modes of the GPP waveguide with width $h/2$ equal to the distance between the plates of the GPP waveguides of the diode and the middle single graphene layer (Fig. 8). Using this equation, we obtain $L_c = 173$ nm which results in transmission of the coupler calculated with FDTD of ~ 0.99 at $\lambda_{\text{opt}} = 9.85$ μm . However, in our design we use $L_c = 130$ nm, since we found that such a coupler length leads to transmission of the coupler of more than 0.93 in a broad wavelength range extending from $\lambda_1 = 9.4$ μm to $\lambda_2 = 13.4$ μm . Using a smaller L_c also decreases the insertion loss. Finally, the distance L_s between the two GPP waveguides of the optical diode (Fig. 8) should be large enough, so that the direct coupling between the modes of the two GPP waveguides is negligible. We note that, if L_f , L_c , and L_s are properly chosen as described

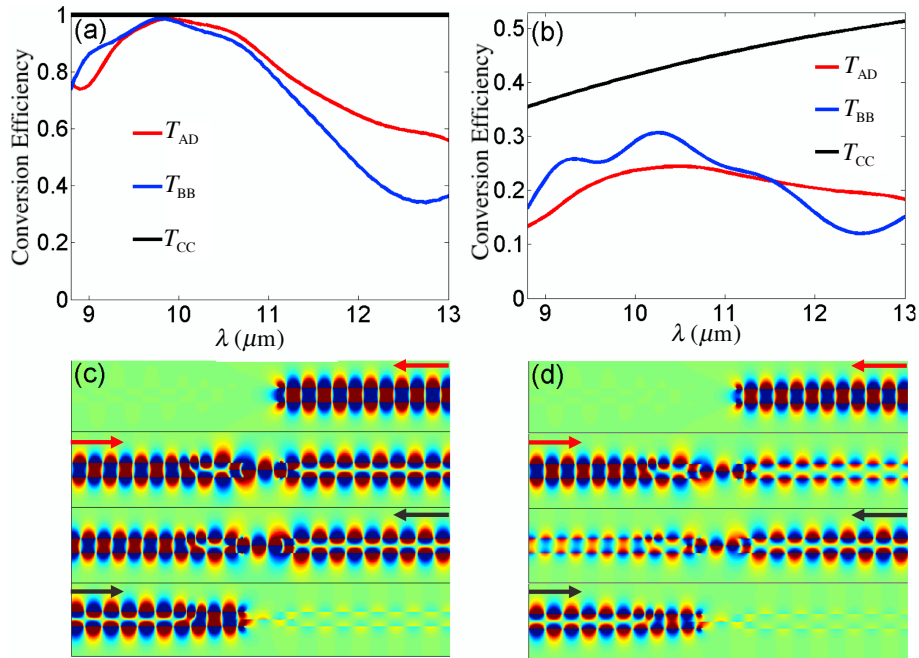


Fig. 9. (a) Transmission spectra from mode A to mode D, and reflection spectra from mode B to mode B and from mode C to mode C calculated with FDTD for the optical diode shown in Fig. 8 with $L = 400$ nm, $L_f = 200$ nm, $L_c = 130$ nm, $L_s = 400$ nm, and $h = 150$ nm. The mode converter of the diode has a chemical potential profile as in Fig. 4(a) with $\mu_{cm} = 0.135$ eV. The graphene layers are assumed to be lossless. (b) Same as in (a), except that the effect of material loss in graphene is included. (c) Magnetic field profiles for the optical diode of Fig. 8 for even and odd modes entering from the left and right directions. The red and black arrows indicate the direction of incidence of the even and odd modes, respectively. The profiles are shown at the wavelength which corresponds to maximum conversion efficiency $\lambda_{opt} = 9.85 \mu\text{m}$. The graphene layers are assumed to be lossless. All other parameters are as in Fig. 9(a). (d) Same as in (c), except that the effect of material loss in graphene is included. When the even mode enters the device from the right, it is reflected, whereas, when it enters the device from the left, it is transmitted. In contrast, the odd mode is transmitted, when it enters the device from the right, and reflected, when it enters the device from the left. This functionality is preserved in the presence of loss.

above, the performance of the optical diode is mainly limited by the mode converter.

The profile for the chemical potential of the mode converter in the optical diode is as the one in Fig. 4(a) with $\mu_{cm} = 0.135$ eV. Figure 9(a) shows the transmission spectra for the lossless case from mode A to mode D, as well as the reflection spectra from mode B to mode B and from mode C to mode C calculated with FDTD. Even though the transmission from mode D to mode A is not shown, we note that it has identical spectra with the transmission from mode A to mode D due to reciprocity [33]. We observe that for the lossless case all coefficients (A to D, B to B, and C to C) are close to 1 at the wavelength at which the diode was designed ($\lambda_{opt} = 9.85 \mu\text{m}$). Figure 9(b) shows the same spectra when the effect of loss is included. When loss is included, there is absorption in the optical diode, which causes the transmission from mode A to mode D to decrease. However, we found that, despite the loss, the structure still acts as an optical diode at the design wavelength λ_{opt} , in the sense that even mode A from the left is only transmitted to odd mode D on the right, while even mode C from the right is only reflected into the same mode C on the right. All other reflection and crosstalk coefficients (A to A, A to

B, A to C, C to A, C to B, C to D) are below -23 dB. Similarly, odd mode D from the right is only transmitted to even mode A on the left, while odd mode B from the left is only reflected into the same mode B on the left. Similar to the even mode case, in the odd mode case all other reflection and crosstalk coefficients (D to B, D to C, D to D, B to A, B to C, B to D) are below -22 dB.

The H_z profiles at $\lambda_{\text{opt}} = 9.85 \mu\text{m}$ for the lossless and lossy cases are shown in Figs. 9(c) and 9(d), respectively. We observe that, when the even mode enters the device from the left, it is transmitted, whereas, when it enters the device from the right, it is reflected. In contrast, the odd mode is transmitted, when it enters the device from the right, and reflected, when it enters the device from the left. This functionality is preserved in the presence of loss [Figs. 9(c) and 9(d)].

4. Conclusions

In this paper, we first introduced a structure that operates as a mode converter between the even and odd modes of GPP waveguides. The converter is reciprocal and is based on spatial modulation of graphene's conductivity. Assuming that the coupling between the two graphene layers of the waveguide is weak, to convert one mode into the other, one needs to create an odd multiple of π phase shift between them. To achieve the required phase shift, we modified the chemical potential on a strip on one of the graphene layers. We first assumed that all graphene layers are lossless. We found that, if the change in the chemical potential on the upper plate is abrupt, the conversion from the even mode on the left to the odd mode on the right at the optimum wavelength is not complete.

To reduce the reflection in such a structure, we used a chemical potential profile that corresponds to a piecewise approximation of a triangular envelope, and found that modifying the chemical potential profile reduces the reflection coefficients of the mode converter to almost zero in a broad wavelength range. In addition, the wavelength of operation of the mode converter can be tuned simply by adjusting the chemical potential of the graphene strip. We also found that the maximum conversion efficiency decreases, when the coupling between the graphene plates becomes stronger. To overcome this issue, we modified the chemical potential of a strip on both the upper and lower graphene plates and found that the double strip converter achieves larger maximum conversion efficiency compared to the single strip converter. When the effect of loss is included, there is absorption in the mode converter, which causes the conversion efficiency to decrease. We found, however, that the functionality of the mode converter is preserved in the presence of loss.

We then introduced an optical diode for GPP waveguides based on a mode converter, and a coupler, which consists of a single layer of graphene placed in the middle between the two plates of two GPP waveguides. As before, we first assumed that all graphene layers are lossless. We found that the existence of the mode converter only on side of the device enables it to perform as an optical diode. When the even mode enters the device from the left, it is transmitted, whereas, when it enters the device from the right, it is reflected. In contrast, the odd mode is transmitted, when it enters the device from the right, and reflected, when it enters the device from the left. When loss is included, there is absorption in the optical diode, which causes the transmission from the even mode on the left to the odd mode on the right to decrease. We found, however, that the device functionality is preserved in the presence of loss.

As final remarks, we note that the proposed devices are based on two-dimensional (2D) GPP waveguides. The corresponding three-dimensional (3D) waveguides, consisting of graphene sheets with finite width, are graphene nanoribbon parallel plate (GNPP) waveguides [48]. Due to the similarity between the symmetric and antisymmetric modes of 3D GNPP waveguides [48], and the even and odd modes of 2D GPP waveguides, we expect that the proposed device designs can also be realized by 3D GNPP waveguides. Fabrication of graphene nanoribbons,

which will be required for the realization of such 3D structures, has been reported by various groups [49–52].

Appendix

Since all graphene layers are suspended in air, we have

$$\epsilon_{r1} = \epsilon_{r2} = 1, \quad (11)$$

$$k_1 = k_2 = k = \sqrt{\beta^2 - k_0^2}. \quad (12)$$

Substituting Eqs. (11) and (12) in Eq. (6) we obtain

$$\beta = k_0 \sqrt{1 - \left(\frac{2}{\eta_0 \sigma}\right)^2}, \quad (13)$$

where $\eta_0 = \sqrt{\frac{\mu_0}{\epsilon_0}}$ is the free space impedance. The surface conductivity of a lossless graphene sheet can be written as follows

$$\sigma = \sigma_{\text{intra}} = \frac{e^2 k_B T}{\pi \hbar^2 j \omega} \left\{ \frac{\mu_c}{k_B T} + 2 \ln \left[\exp\left(-\frac{\mu_c}{k_B T}\right) + 1 \right] \right\}. \quad (14)$$

At room temperature ($T = 300$ K), $k_B T \cong 26$ meV and, since the applied chemical potentials in this paper are larger than 100 meV, we have $2 \ln \left[\exp\left(-\frac{\mu_c}{k_B T}\right) + 1 \right] \ll \frac{\mu_c}{k_B T}$. Consequently, we obtain

$$\sigma \cong \frac{-j e^2 \mu_c}{\pi \hbar^2 \omega}. \quad (15)$$

Substituting Eq. (15) into Eq. (13) we obtain

$$\beta = k_0 \sqrt{1 + \left(\frac{2\pi \hbar^2 \omega}{\eta_0 e^2 \mu_c}\right)^2}. \quad (16)$$

For the range of wavelengths considered in this paper we have $\left(\frac{2\pi \hbar^2 \omega}{\eta_0 e^2 \mu_c}\right)^2 \gg 1$. Therefore, Eq. (16) can be simplified as follows

$$\beta = k_0 \left(\frac{2\pi \hbar^2 \omega}{\eta_0 e^2 \mu_c}\right) = \frac{2\pi h^2}{\mu_0 e^2} \frac{1}{\mu_c \lambda^2}. \quad (17)$$

Using Eq. (17), the propagation constants for the i^{th} segment of the upper and lower plates are

$$\beta_{ui} = \frac{2\pi h^2}{\mu_0 e^2} \frac{1}{\mu_{cui} \lambda^2}, \quad (18)$$

$$\beta_{di} = \frac{2\pi h^2}{\mu_0 e^2} \frac{1}{\mu_{cdi} \lambda^2}, \quad (19)$$

where μ_{cui} and μ_{cdi} are the chemical potentials of the i^{th} segment of the upper and lower plates, respectively. Substituting Eqs. (18) and (19) into Eq. (10), the wavelength of maximum conversion efficiency λ_{opt} can be calculated as follows

$$\lambda_{\text{opt}} = \sqrt{\frac{2h^2}{(2m-1)\mu_0 e^2} \left[\sum_{i=1}^N d_i \left(\frac{1}{\mu_{cui}} - \frac{1}{\mu_{cdi}} \right) \right]}. \quad (20)$$

The values of μ_{cui} , and μ_{cdi} depend on the the minimum potentials μ_{cmu} , and μ_{cmd} of the corresponding triangular envelopes [Fig. 4(a)]. We verified that Eq. (20) gives results indistinguishable from those obtained using Eq. (9).

Funding

National Science Foundation (NSF) (Awards No. 1102301 and 1254934).